Composite Structures 131 (2015) 193–206

Contents lists available at ScienceDirect

Composite Structures

journal homepage: www.elsevier.com/locate/compstruct

Reaction forces of laminated glass windows subject to blast loads

P. Del Linz [a,1], P.A. Hooper [a,*], H. Arora [a], D. Smith [b], L. Pascoe [b], D. Cormie [b], B.R.K. Blackman [a], J.P. Dear [a,*]

[a] Imperial College London, Department of Mechanical Engineering, Exhibition Road, London SW7 2AZ, United Kingdom
[b] Arup Resilience Security and Risk, 13 Fitzroy Street, London W1T 4BQ, United Kingdom

ARTICLE INFO

Article history:
Available online 5 May 2015

Keywords:
Laminated glass
DIC
Blast
Reaction forces

ABSTRACT

Several blast trials on laminated glass windows have been performed in the past, using both full field 3D Digital Image Correlation and strain gauges located on the supporting structure to collect information on the glass pane behaviour. The data obtained during three blast experiments were employed to calculate reaction forces throughout the perimeter supports both before and after the fracture of the glass layers. The pre-crack experimental data were combined with finite element modelling results to achieve this, whilst solely experimental results were employed for post-cracked reactions. The results for the three blast experiments were compared to identify similarities in their behaviour. It is intended that the results can be used to improve the existing spring–mass systems used for the design of blast resistant windows.

1. Introduction

The blast protection of buildings and infrastructure is of high importance in modern society due to the threat of both terrorist and accidental explosions. The design of glazing systems including both windows and facades is key to maximising the overall robustness and resilience of structures.

Polyvinyl Butyral (PVB) laminated glass has been found to offer a much higher level of protection than monolithic glass and significant research has been conducted to improve the understanding of its behaviour. Several experiments were performed subjecting laminated glass panes to blast loads. Amongst these, Hooper et al. [1] and Stephens [2] performed blast trials measuring the deflections of laminated glass panes. Wei and Dharani [3,4] took a theoretical approach and carried out studies using von Karman large deflection theories and Griffith fracture energy balance to estimate the behaviour of the glass plies before and after glass cracking occurs. Kumar and Shukla [5] compared experimentally laminated glass with other systems, such as tempered glass and wired glass. A shock tube was used to load the samples. The authors concluded that the laminated glass samples resisted the loads most effectively, especially when combined with protective films.

Whilst several recent studies were conducted to develop finite element models able to represent the whole behaviour of a glass pane under blast loads [6,7], historically the single degree of freedom (SDOF) model has been used as a simplified tool to produce designs within acceptable cost and time scales [8]. In this approach, the complex system of the laminated glass and its connections to the supports is approximated with an appropriately damped mass–spring model. Failure is considered to occur when a system limiting deflection is reached.

The loads imposed on a window frame by the glass are critical in the design of blast resistant facades. The window pane, usually laminated, should resist a prescribed blast without failure, but it is equally important that the loads from the pane edges should be carried without failure by the sealant, the rebates, the frame itself and its fixings to the support structure. Experience has shown that any kind of window failure can be followed by extreme devastation and human injury inside the building.

To calculate the support reactions with the SDOF method a spring force–displacement relationship (resistance function) is required. This represents the system internal forces resisting the displacement of the degree of freedom. Under the application of a static load, the reactions from the spring–mass system would be equal to the externally applied force and would result in sufficient displacement of the spring such that internal and external equilibrium is achieved [9]. Besides this limiting case, for simple systems, such as a beam undergoing small amplitude vibrations,

* Corresponding authors. Tel.: +44 (0)20 7594 7128; fax: +44 (0)20 7594 7017 (P.A. Hooper). Tel.: +44 (0)20 7594 7086; fax: +44 (0)20 7594 7017 (J.P. Dear).
E-mail addresses: paul.hooper@imperial.ac.uk (P.A. Hooper), j.dear@imperial.ac.uk (J.P. Dear).
[1] Present address: School of Civil and Environmental Engineering, Nanyang Technological University, 50 Nanyang Avenue, 639798, Singapore.

http://dx.doi.org/10.1016/j.compstruct.2015.04.050
0263-8223/

the resistance function can also be calculated directly from structural dynamics principles.

However, characterising the response of a window subjected to blast loading, and subsequently to cracking, is much more complex. At present, a shape for the resistance function is assumed and calculations are performed with reference to previous experiments to determine limiting values for resistance and displacement [8]. Factors can then be applied to the resistance and the externally applied force to produce estimates of the reactions on each of the four window sides [9]. Several resistance functions have been proposed in the past. Smith [8] proposed a linear resistance function after glass cracking. Fischer and Häring [10] also conducted analysis of blast experimental data attempting to fit linear resistance functions. They then compared the deflections obtained from single degree of freedom models with those obtained during the experiments. They concluded that a tri-linear function yielded a reasonable representation of the deflections observed during the experiments.

In the present study, data from Hooper et al.'s blast experiments [11] were used to determine the reaction forces directly, as it was felt that these data would assist in producing more accurate SDOF models. Digital Image Correlation (DIC) data were used to estimate the deflection and strains at all points across the laminated glass pane. In the three blast trials considered here pairs of strain gauges were placed on the supporting frame to measure elastic strains within the steel supporting frame. These combined data were employed to calculate reactions along the window edges both before and after the glass failure. This information was then evaluated and the different results for the experiments considered were compared. The reaction data found in this way can also be employed to improve the resistance function estimates, ultimately providing a more precise tool for window design.

Table 1
Summary of main blast parameters of the experiments considered.

Experiment	Charge weight (kg)	Stand-off (m)	Peak reflected pressure (kPa)	Impulse (kPa ms)
1	15	13	140	284
2	30	16	132	413
3	30	14	152	461

2. Method

Hooper et al. [1] performed eight full-scale blast trials on laminated glass. Three of these were employed in this study and were labelled Experiment 1, Experiment 2 and Experiment 3. The make-up of the panes was two 3 mm thick plies of annealed glass with a 1.52 mm PVB interlayer. The explosive charges were 15 and 30 kg and the stand-offs were as in Table 1.

Fig. 1 shows a typical layout of the test pad. Other cubicles were generally present, however they were located so as to avoid blast wave reflections during the first part of the experiment. The locations of the pressure gauges are also shown in the sketch. In Experiment 1, a gauge was set up to record the incident pressure wave at the same stand-off as the sample. In Experiment 2 and 3 instead pressure gauges were fixed to a large concrete block to collect reflected pressures [11].

During all three experiments Digital Image Correlation techniques (DIC) were employed to provide 3D full field information on deflections and strains in all directions. Two Photron S3 cameras were used to take images of the window at 1 ms intervals. Two window panes were tested side by side in the same cubicle. Slightly different boundary conditions occurred on the two outer vertical sides of the windows due to leakage of blast pressure at the cubicle edges. This effect was counteracted by an increased flexibility at the central edges due to the cubicle construction. Fig. 2 shows the typical DIC set up used.

Typical results for deflections and strains are shown in Fig. 3. Similar results were available at each time step for all the cases considered.

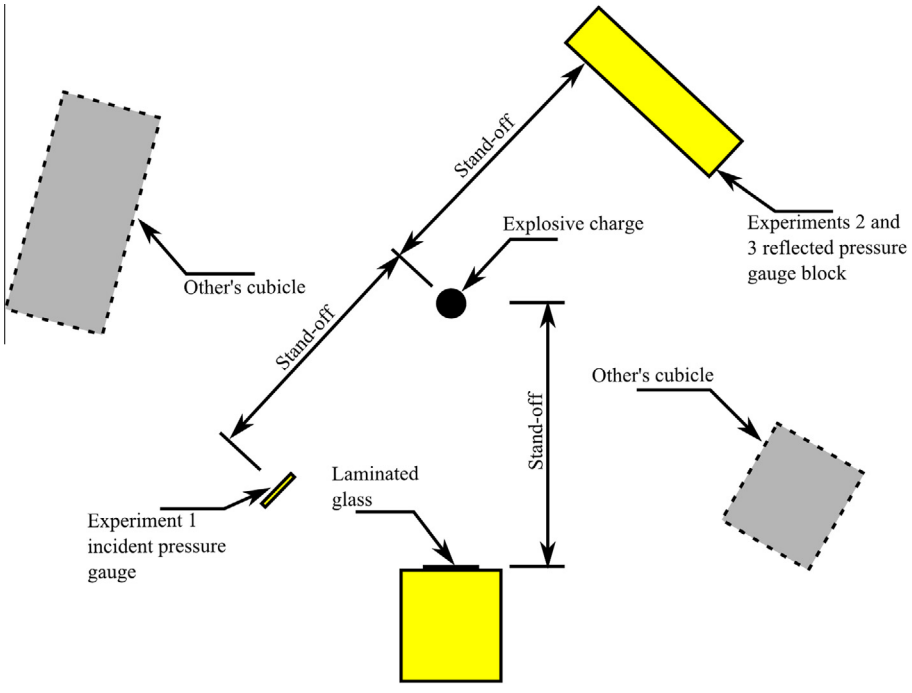

Fig. 1. Plan view of the test pad. The locations of the specimen and of the pressure gauges are shown. The stand-off distances varied between experiments.

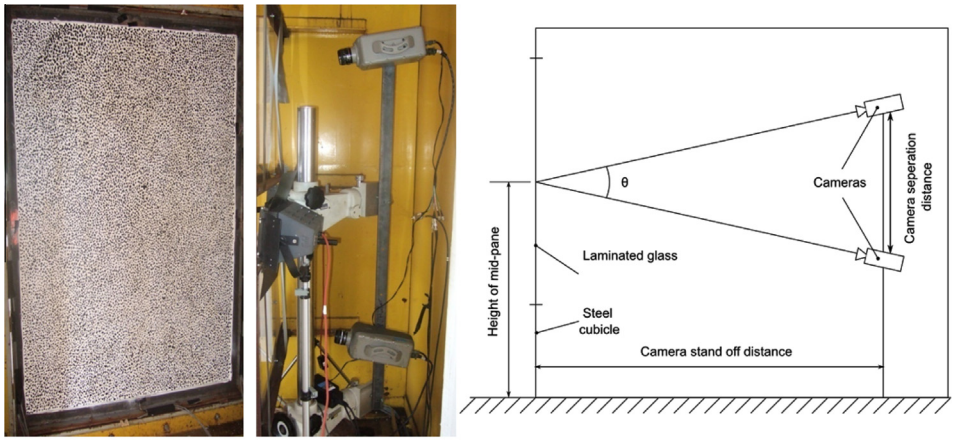

Fig. 2. DIC set up used in Hooper et al.'s blast experiments (adapted from [1]).

All the experiments included four pairs of strain gauges located at the centre of each window side on the supporting steel angles of the frame. These were used to measure the local reaction force.

For all three experiments, the available 3D deflection and strain data was interpolated at regular grid points. It was found that as the deflections increased the layout of the stereoscopic cameras and the processing software were unable to provide data for a growing band of facets along the edges of the glass pane. An extrapolation technique was therefore used to obtain the out of plane deflections for these facets.

This extrapolation involved fitting a 4th order polynomial surface to the available data. Afterwards, the data were substituted by the fitted results either where the experimental deflection values were not available or where they presented unrealistically high positive or negative data points along the edges.

Whilst it would have been ideal to apply the same technique to the experimentally derived strain data, their more variable nature prevented an acceptable fit being achieved. It was therefore concluded that extrapolated points would not be realistic.

All the blast experimental data obtained were employed to calculate reactions of both the pre-cracked and the post-cracked pane. Due to the different behaviour of the glass in the two situations, separate approaches were employed as outlined below.

2.1. Pre-crack reactions

In the pre-cracked phase (glass responding elastically prior to fracture), the applied blast loading will generate a combination of out-of-plane bending and shear, and in-plane membrane stresses within the window pane. Soon after the blast wave reaches the target, as the deflections will be small, membrane forces will be negligible in accordance with traditional small deflection theory. However, the window can deflect significantly compared with its thickness before cracking takes place. For example, in the experiments considered here, the central deflection generally reached up to 40 mm before the glass fractured. At these levels of deformation small deflection theory assumptions are no longer valid and a non-linear analysis considering in-plane membrane forces is required. Fig. 4 shows the forces which will be generated in this phase of the loading.

As the DIC data were collected for only one face, the bending and membrane stresses could not be distinguished directly. Their relative magnitude at each point of the window was estimated using finite element modelling. The model was used only to obtain the relative proportions of these strains, which were then applied to the experimental DIC data for further analysis. A pre-cracked FEA model similar to that developed by Hooper [1] was employed. However, the simulation was developed further by including additional elements. These included the steel support structure and a layer of silicone between the glass and the supports. The model was developed using ABAQUS 6.9 [12]. The laminated glass was represented with 2D shell stress elements using reduced integration. The section was defined as a layered composite, using the real thicknesses of the three layers (3 mm for the glass plies and 1.52 mm for the PVB). The elements were generally of square shape, with a side length of 2 mm at the silicone interface and 4 mm elsewhere. A mesh size sensitivity analysis was run and elements of this dimension were found to be small enough to avoid size effects.

Steel 100 mm equal angle supports were used in the blast experiment and therefore were added to the analysis model. Again, 2D reduced integration shell elements were employed for these. The element dimension varied between 2 mm in the areas of contact with the silicone and 4 mm in other areas. A uniform material section was used, setting the thickness to 6 mm. The layer of silicone was included using 3D stress elements with reduced integration. This was considered necessary due to the high through thickness deformation expected in this material. Cubic elements were used, with a side length of 2 mm. The overall silicone thickness assumed was 6 mm, with a bite depth of 20 mm. Three elements where therefore used across the thickness to achieve the necessary quality of through thickness results. Tie conditions were set between the different parts, without any allowance for sliding.

The glass, PVB and steel were all modelled as linear elastic materials. Both the steel and the glass would behave linearly in the range of deformation of interest. Whilst the PVB would be likely to show some non-linearity, its much lower stiffness implies that its contribution to load resistance can be considered negligible prior to the failure of the glass layers. Hence, for simplicity, it was also considered acceptable to employ a linear model for this element. Table 2 summarises the constants used for these three materials.

Due to the expected large displacements, the silicone was instead represented using a hyperelastic material model. A

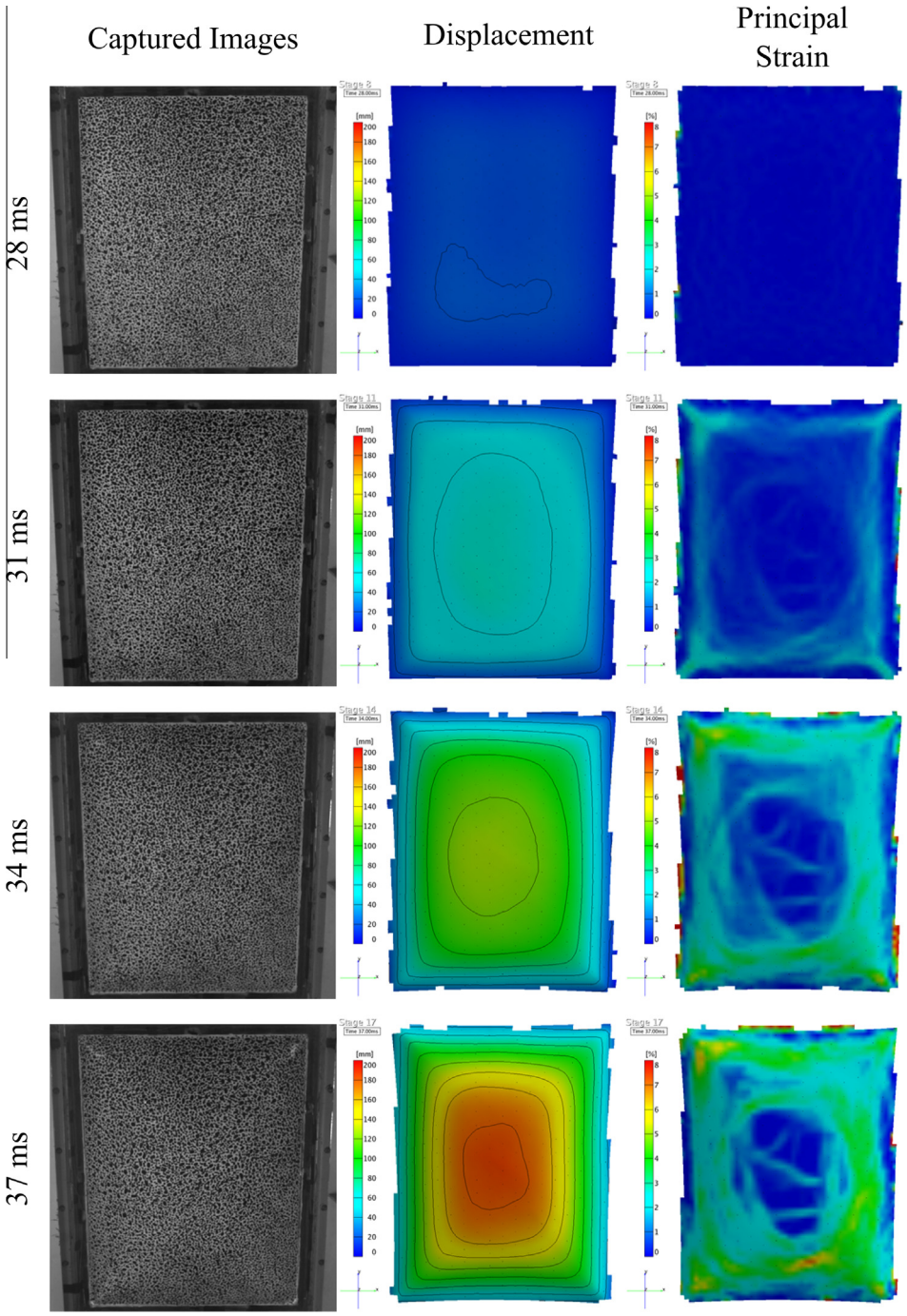

Fig. 3. Typical DIC results from a blast experiment. Both the out of plane deflections and major strains are shown (adapted from [1] – Time = 28 ms is the onset of deformation).

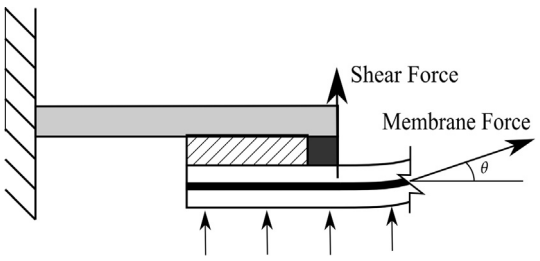

Fig. 4. Representations of the reactions assumed in the pre glass cracking force calculation.

Table 2
Summary of linear elastic material properties applied in the FEA models.

Material	Material density (kg/m^3)	Young's modulus (GPa)	Poisson's ratio
Glass	2530	72	0.22
PVB	1100	0.5	0.485
Steel	7800	200	0.3

Mooney–Rivlin model was used, which is able to represent the non-linear elastic deformations of rubber-like materials. The work function is given by [13]:

$$W = C_{mr1}(I_1 - 3) + C_{mr2}(I_2 - 3) \quad (1)$$

where W is the work done by the deformation, I_1 and I_2 are the invariants of the deformation tensor and C_{mr1} and C_{mr2} are materials stiffness parameters determined from the experimental data. The constants used were derived by Meunier et al. [14], with values of C_{mr1} = 0.14 and C_{mr2} = 0.023 MPa.

The blast load was applied as a uniformly distributed pressure over the whole glass pane and the supports. The pressure time history was estimated from computation fluid dynamics (CFD) models of the experiments. It was decided to not use the experimentally recorded pressure as the gauges were not located in the same position as the experimental sample. Additionally, comparisons between the two sets of pressure data and the DIC observations generally showed the calculated blast wave characteristics to be more realistic in terms of arrival time and pressure magnitude [11]. The Air3D [15] analysis code was used for this. This produced pressure estimates at 0.0001 s intervals at points on a 50 × 50 mm grid on a quarter of the window. It was observed that the pressure on the glass varied only by 10% over the whole area. Considering this and the fact that the FEA model would be used to find only the ratio of bending and axial stresses, it was decided that an average pressure at each time step would be appropriate for this application. This was therefore calculated from the Air3D output and used within the FEA model.

The model was set to run until a limiting principal tensile stress of 80 MPa was reached in any of the glass elements. This stress value was used as an estimate of the likely fracture stress of glass subject to dynamic loading [16]. As a checking procedure, the central deflection was also compared with the recorded experimental data. The strain data were then extracted and the relative proportions of bending and axial strains were calculated. The experimental DIC strain data were then multiplied by these proportions, producing both bending and membrane strains to be used in further calculations.

Once the experimental bending strains were found, the bending stresses and hence the moments were calculated along sections at 20 mm intervals in both directions. The shear force was then determined by numerically differentiating the moments with respect to the distance along the window's span. It was then assumed that the out of plane reaction due to the bending moment at the edges would be equal to the magnitude of the shear force. As the strain data were found to be quite noisy, they were filtered to obtain a smoother output.

It was assumed that the glass could not resist tensile stresses higher than 80 MPa, therefore if a stress higher than this was found in the data it was reduced to 80 MPa. Fourier transforms were then employed to filter some of the noise, eliminating higher order frequencies from the data set. Additionally, an average of the last three points of the bending moment diagram slope was employed when calculating the reaction force. The results at each facet were then numerically integrated to calculate the total reaction force along the edges of the window.

The DIC membrane strains were converted to stresses using the same linear elastic model for the glass used in the FEA model. Again, Fourier transforms were employed to reduce the noise in the data and an average of the last three data points near each edge was taken to obtain edge stress values. To calculate the total membrane force at each point, the stress was multiplied by the glass plies thickness, as it was considered that the stiffness of the PVB was much smaller and would provide only a very small contribution to the overall result.

The calculated force would be acting in the plane of the glass. To estimate the in-plane and out-of-plane components, the glass angle at each time step was calculated using the out-of-plane deflection data at each facet. The membrane reaction was therefore split and the out-of-plane component were added to the bending reaction calculated previously.

2.2. Post-crack reactions

After glass cracking takes place, it is assumed that no bending stiffness will be left in the laminated glass and that the blast force will be resisted entirely by membrane action of the PVB. Hooper et al. [1] developed a method to calculate the reaction force on the frame at the strain gauge locations. This employed the data from the strain gauge pairs and the glass angle at the frame was then calculated from the out-of-plane deflection DIC data. The geometry of the system is as shown in Fig. 5.

The strains at the gauge locations (ε_1 and ε_2) were known, as were all the geometrical properties. In this case L was 31 mm, H was 12.75 mm and T was 6.00 mm. Whilst in theory data from the gauges would provide sufficient information to determine both the axial and bending forces, in practice the system's sensitivity to misalignment of the gauges proved too high to reliably calculate both the bending moment and the axial force using solely their data.

Hooper et al. showed that misalignment errors have a more significant effect on the axial force component estimate than on the bending moment. The DIC records provided the time varying angle of the reaction force and allowed the membrane force in the pane to be calculated by considering only the equation for the bending moment component. Employing basic stress analysis principles and some manipulation, Hooper obtained the final equation:

$$F = \frac{\varepsilon_b \times E \times T^2}{6 \times (\cos(\theta) \times H + \sin(\theta) \times L)} \quad (2)$$

where E is the Young's modulus of steel, T, H, F, θ and L are defined as shown in Fig. 5 and ε_b is the bending strain, which is given by:

$$\varepsilon_b = \frac{\varepsilon_1 - \varepsilon_2}{2} \quad (3)$$

To calculate reaction forces at points along the edge away from the location of the strain gauges, a material model linking the recorded DIC strains and stresses in the laminate was required. In this research such a material model was fitted at each strain gauge pair location and then applied along the edge on which the pair was located.

The described formulae were employed to find local reaction forces at the gauge locations. This was then divided by the PVB thickness, providing the stresses in the interlayer at each time point. The DIC strains at the locations nearest to the gauges were then extracted, averaging the results over an area of 3 × 3 facets to reduce the effects of noise. This enabled a stress strain curve to be plotted for each edge, and a chosen material model to be fitted using a least squares difference approach.

As the cracked laminate stress–strain data showed that the stress reached a plateau after an initial stiff linear increase, a plastic material model was used to represent the composite material. This model does not reflect a physical characteristic of the cracked glass-PVB laminate material. However, for the purpose of this analysis, such a model was useful as it captured the shape of the observed data. In keeping with the method applied by Hooper et al. for their FEA models, a Johnson–Cook [17] model was used. Since a plasticity model was only used to represent the observed shape of the data, employing more sophisticated, physically based formulations would not represent an improvement on this simple model.

As in the experiments the strain rate could not be controlled and the noise in the data precluded its accurate estimate, the corresponding portion of the model was not employed. The constitutive equation used was:

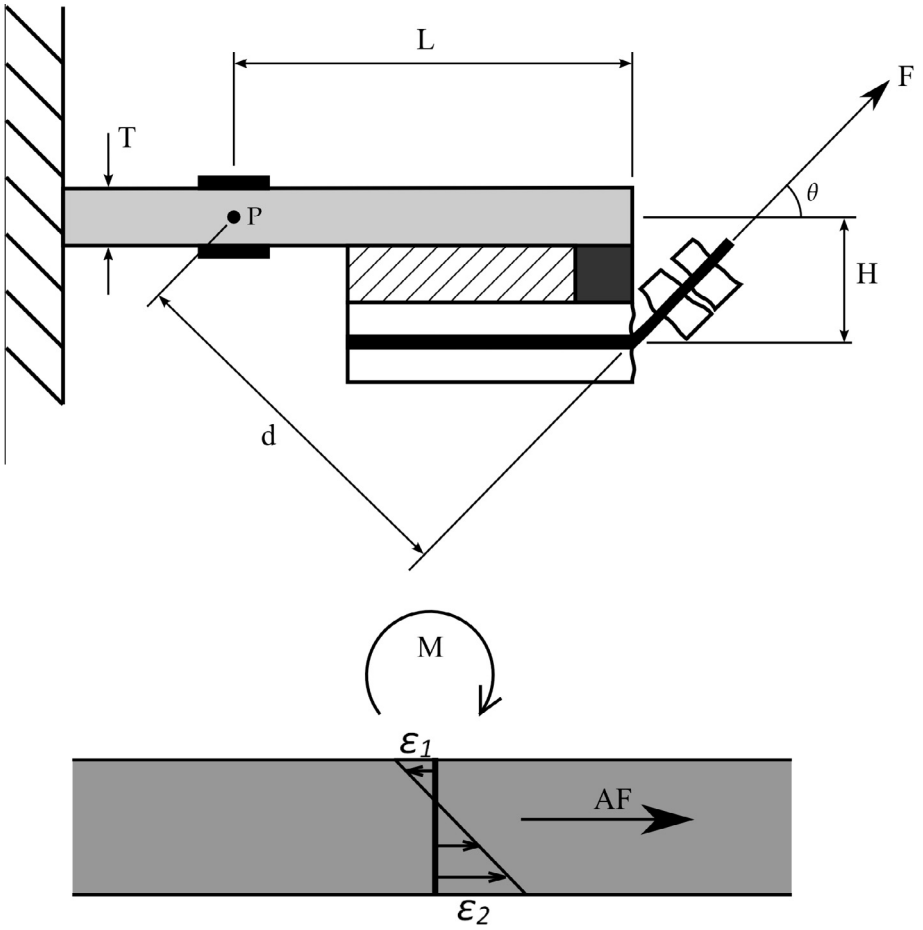

Fig. 5. Geometry used for the calculation of the reaction forces at the strain gauge locations. Both the applied forces and the bending and axial strains are shown. Figure adapted from Hooper et al. [1].

$$\sigma = (A + B\varepsilon_p^n) \tag{4}$$

where A, B and n are constants to be determined and ε_p is the plastic strain.

Once the model was calibrated, the stress levels at each point could be obtained, allowing the calculation of the membrane force throughout the pane perimeter. Again, the glass pull angle was calculated at each point along the edge to split the total reaction force in the glass into out of plane and in plane reactions in the frame.

2.3. Energy estimates

The post-crack reaction forces results and the experimental data were used to estimate the internal strain and kinetic energies in the laminated windows. The kinetic energy could be calculated directly using the known mass of the window per unit area and the velocity data for each facet obtained from the DIC analysis. The results could then be integrated over the window surface. The internal strain energy was found by assuming the reactions along the edges indicated the average stress in the PVB membrane. To calculate this, the reactions at each point on the two opposite window sides were averaged. The result was then divided by the PVB area to find the average stress, which was assumed to be constant throughout the section being considered. This result was then used together with the strain DIC results to calculate the internal strain energy.

The pressure recordings were employed to calculate the external work done on the samples. The pressure acting on each DIC facet was multiplied by the facet area to obtain a local force. The force deflection curves were then numerically integrated to find the external work.

With this information, an estimate of the energy absorbed by the glass cracking and other energy loss processes was produced for each experiment by subtracting the sum of the kinetic energy and internal strain energy from the external work.

The total energies associated with the explosions were also calculated. The energy released by the explosive material was assumed to be 247.9 kcal/mol of equivalent TNT [18], with a mole of TNT equal to 227.13 g. A spherical and a hemispherical blast fronts were utilised to calculate the energy per unit area at the experimental stand-off distances. These were considered to be the two limiting cases, as they represent the boundary conditions of a perfectly absorbing and a perfectly reflecting ground. The dimensions of the glazing panes were then used to calculate the total energy which could be potentially transferred to the samples.

3. Results

3.1. Pre-crack reactions

As discussed, the proportions of surface strains due to out of plane bending and in plane membrane forces were calculated using a FEA model of the glass pre-cracking phase. Fig. 6 shows a sample plot of the central deflection time history obtained from the FEA model and the DIC data for Experiment 2. The trends of the FEA and experimental deflections were similar in the range

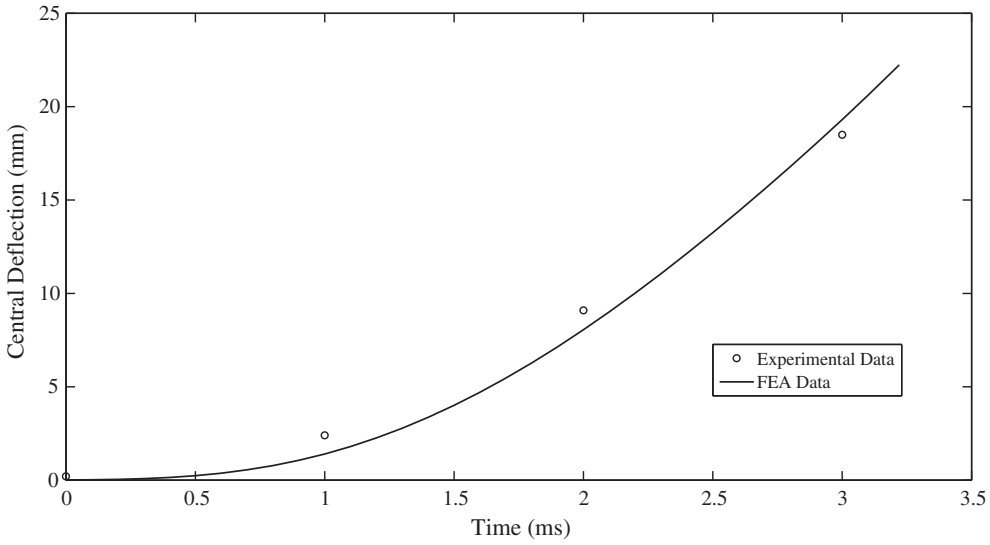

Fig. 6. Comparison of central deflection obtained through DIC and FEA modelling for Experiment 2 (Time = 0 ms is the blast wave arrival time). Measurement uncertainties are not shown for the DIC experimental data as they were too small to be evident at the graph scale.

of interest. In the FEA data shown in the image, the central deflection reached at the glass cracking condition was 22.2 mm, which was compatible with recorded values, in which failure took place between 18.5 and 32 mm. This comparison of the measured and estimated failure deflections produced similar results for all experiments considered.

Fig. 7 presents the proportion of stresses due to bending moments and membrane forces found through the FEA model for Experiment 2 as an example. The proportion of bending strain was found to be higher towards the edges of the panel, whilst it decreased to almost zero in the central area. The membrane proportion shows the opposite behaviour, rising significantly in the centre of the window.

These proportions were applied to the recorded DIC strains, and the strain along each cut in both directions considered in turn. As described previously, the data so obtained were filtered to improve the shear force estimate. Fig. 8 shows a typical plot of the bending stresses along a cut, showing the original data and the filtered result.

The plot shows that the maximum bending strains are reached near the supports, tapering to the lowest values towards the centre of the panel. This behaviour is typical and can be seen throughout the specimens, although it becomes more pronounced as the time increases. The membrane stresses were calculated using the same filtering techniques.

The overall out-of-plane reactions calculated along one of the edges are presented in Fig. 9. The membrane force component is close to zero in this time frame, although it increases as the loading progresses.

The overall reaction results will be shown below in Figs. 14 and 15 together with the post crack reaction results.

3.2. Post crack reactions

The material model for the cracked laminate was fitted to tensile stress strain curves produced with the method described previously. A typical curve together with the data fit is shown in Fig. 10.

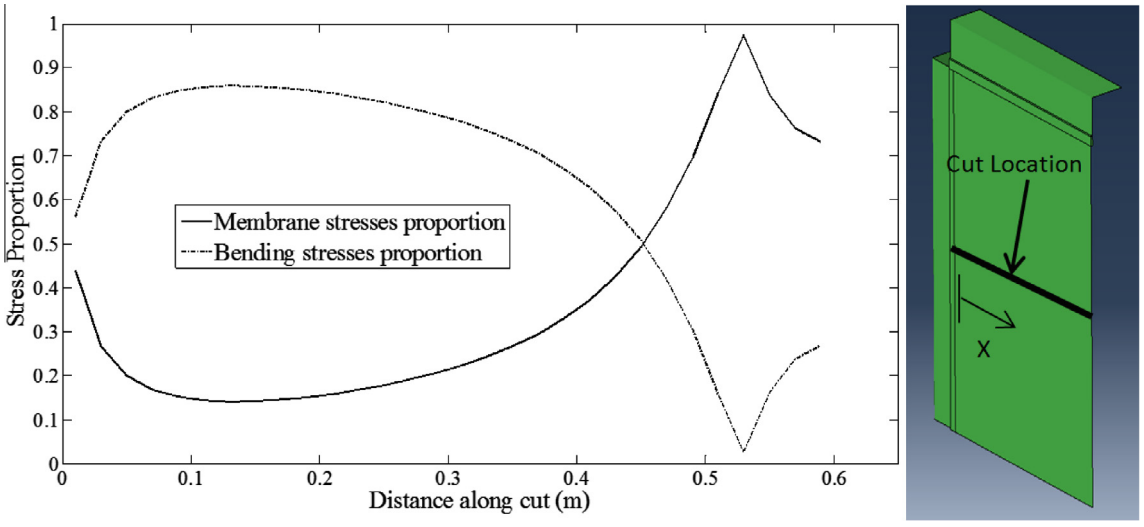

Fig. 7. Proportion of the stresses due to bending moments and membrane forces just before glass failure found with the FEA model for Experiment 2.

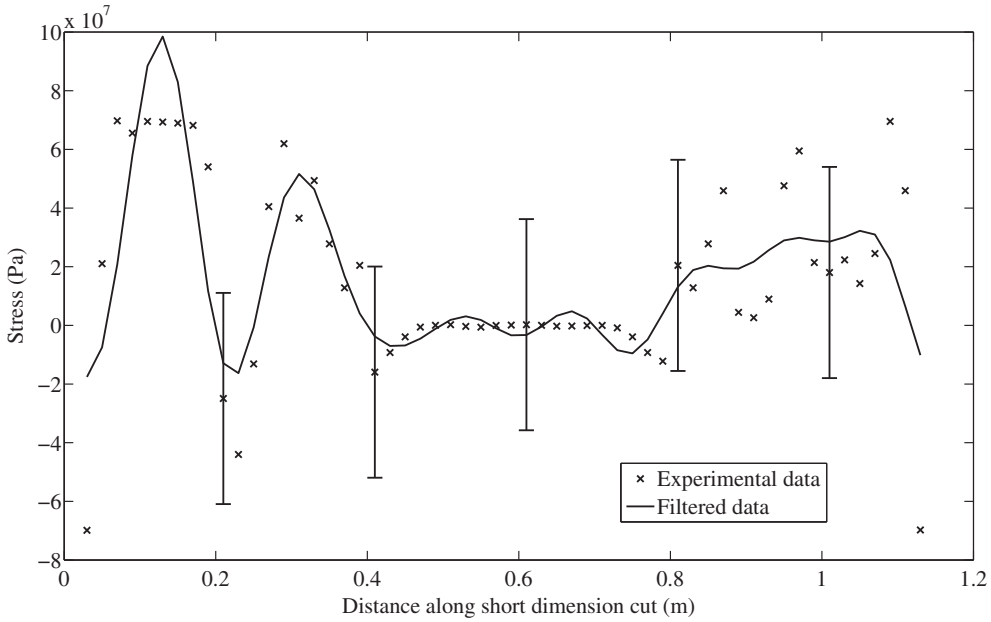

Fig. 8. Samples of bending stress data. Both the original DIC data and the filtered curve are shown. DIC uncertainties of 0.1% were assumed to plot the data error bars. The error bars were plotted at only a few points for clarity.

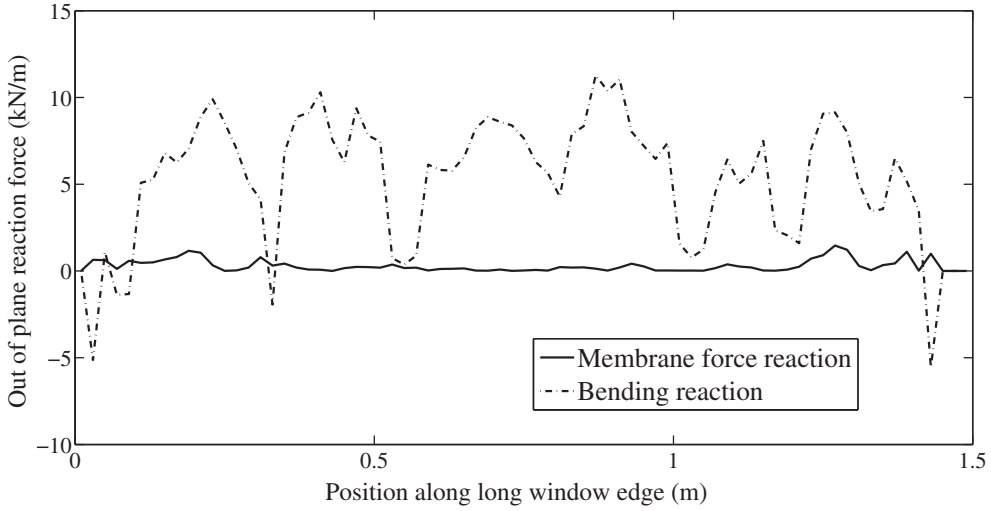

Fig. 9. Out-of-plane reaction force along one edge. The bending and membrane components are shown separately.

As can be seen, the data were noisy. Additionally, for two panel edges in Experiment 1, data uncertainties prevented a reliable estimate of the material coefficients. Where this happened, the material models calculated for the opposite window side on the same experiment were employed, as it was decided that these locations would present the most similar behaviour. However, wherever possible the model fitted to the actual data was retained. It was decided that the variation in these models was caused by differences in the behaviour of the cracked material and of the system at the different locations. Therefore, the discrepancies were taken into consideration for the latter stages of the analysis. Table 3 shows the Johnson–Cook material model coefficients obtained for Experiment 2 as a typical example.

These models were employed on their respective sides to calculate the reactions at all points. Fig. 12 shows a plot of the reactions along an edge of one of the windows at two time steps. The reactions seemed to reach two maxima near the ends of the window side.

The data were used to find edge reactions in the plane of the glazing. Fig. 13 shows the total reactions generated on all four sides for each of the three experiments. It can be seen that the reactions are substantially constant throughout the range of displacements. These data were then converted to in-plane and out-of-plane forces with the DIC edge angles.

Fig. 14 shows the out-of-plane reactions on each side of the glazing panel during Experiment 2. The legend of the edge locations is shown in Fig. 11. It can be seen that the forces reached an initial during the pre-cracked phase, at a central displacement of approximately between 20 and 30 mm. After falling they increased again, reaching a plateau level at higher displacements.

The total out-of-plane reactions for all experiments are compared in Fig. 15. The pre-cracked reactions peaked between 32

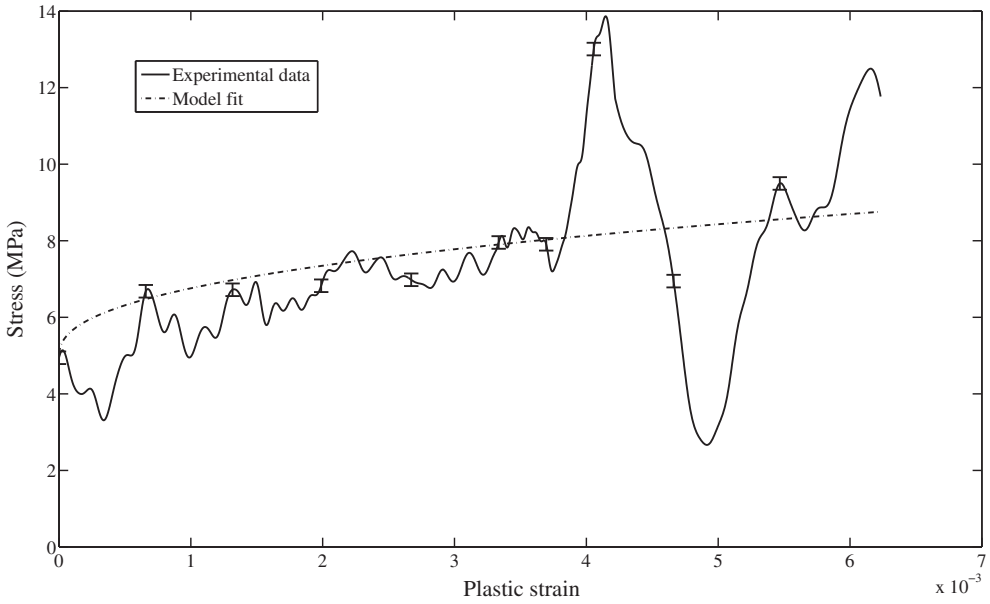

Fig. 10. Stress strain curves for the estimate of cracked glass material model. The errors calculated by Hooper [11] were used for the experimental stress. Only a few error bars were plotted for clarity.

Table 3
Johnson Cook fit coefficients for Experiment 2. The results for each window side are shown. Refer to Fig. 11 for a legend of the side locations.

Side	Johnson–Cook parameters		
	A (MPa)	*B* (MPa)	*n*
Top	6.58	4.32	0.11
Bottom	11.44	28.72	0.62
Wall	12.73	9.88	0.17
Central	5.62	8.7	0.14

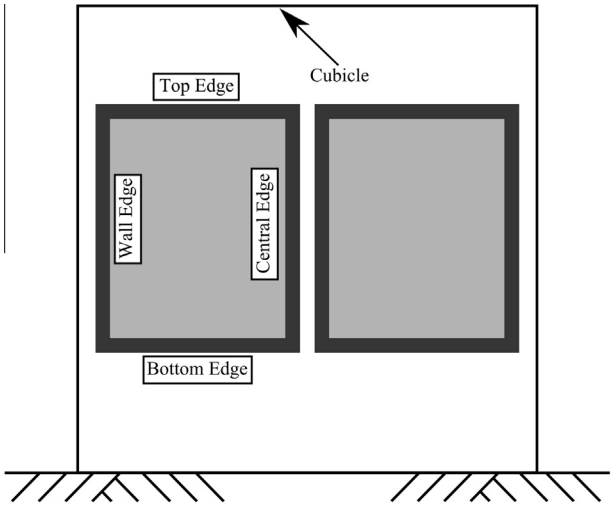

Fig. 11. Edge location legend.

and 45 kN. The post-cracked reaction magnitude instead varied to a greater degree between the experiments, ranging between 31 kN in Experiment 2 and 53.4 kN in Experiment 3 due to the greater loading in this last experiment. In all cases the reaction force approached a plateau level.

The in-plane forces were also considered. For these, pre-cracked reactions were ignored. They would be dependent only on the small membrane forces present, and noise would have prevented achieving a realistic estimate. The results showed a somewhat different behaviour. A plateau level was reached as in the out-of-plane case, however the rise time was very short and the forces were significantly more consistent as the deflection increased.

Fig. 16 presents the total in-plane force results for all the blasts considered. As mentioned, the rise time of the reactions was lower than the time difference between the images, 1 ms, after the failure of the glass. The line fits show a slight decrease in the loading as the experiment progresses. However, this effect is limited, with a maximum decrease of 7.7 kN, 8.8%, in the greatest case, Experiment 3.

The out-of-plane pre-cracked peak forces and plateau levels and in-plane plateau levels are summarised in Table 4.

3.3. Energy estimates

The post-crack results were used to calculate the internal strain energy for each experiment. The kinetic energies and external work done were also calculated for each time step. Fig. 17 shows typical results, obtained in this case for Experiment 2. In general, the strain energy magnitude was relatively small compared to the kinetic energy. The external work was significantly larger than both these measures, indicating that irreversible deformations, such as the glass cracking, absorbed a large amount of energy.

The results for all three cases are shown in Table 5, whilst the total blast energy comparison is shown in Table 6. The results showed that the internal strain energy developed was relatively constant between the experiments. Instead, the kinetic energy and external work done increased significantly with increasing blast intensity. As a result of this the proportion of energy absorbed by irreversible deformations seemed to decrease as the blast energy increased. The work done is significantly smaller than the blast energy, with the largest ratio in Experiment 3 being 6.8%. The energy absorbed by delamination and cracking is therefore also small compared to the total, with 3.1% in Experiment 2 being the largest proportion.

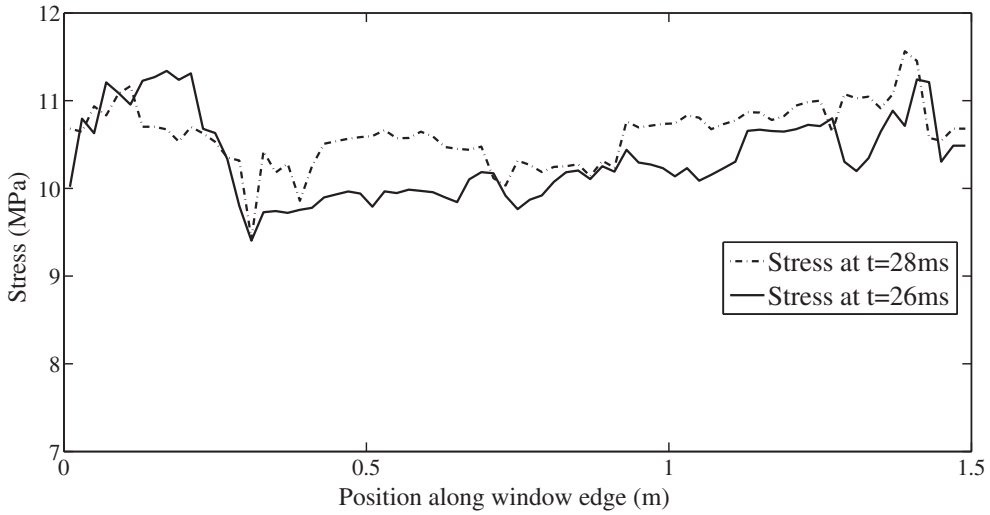

Fig. 12. PVB reaction stress along the bottom edge of Experiment 1 at time steps $t = 26$ and $t = 28$ ms.

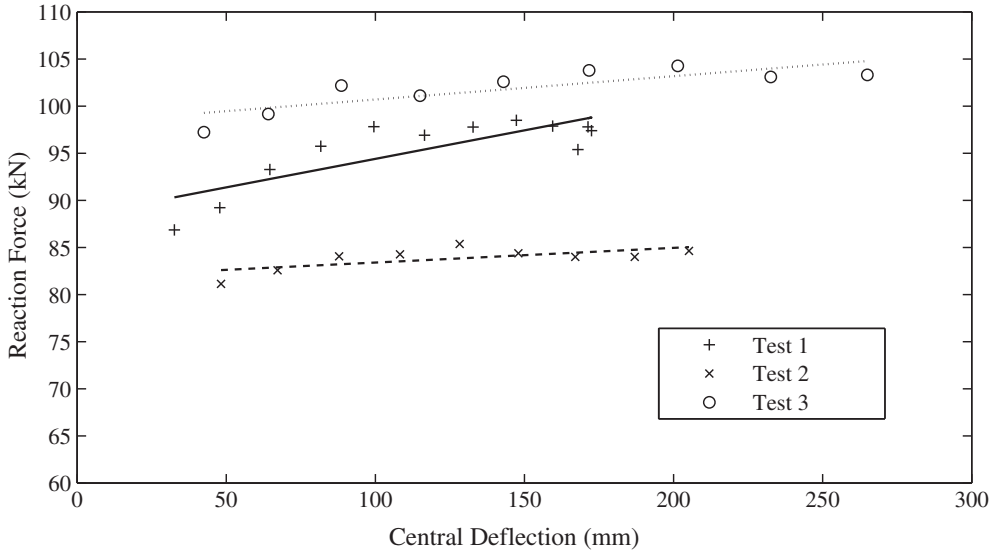

Fig. 13. Total post-cracked reactions forces in the window plane for all experiments.

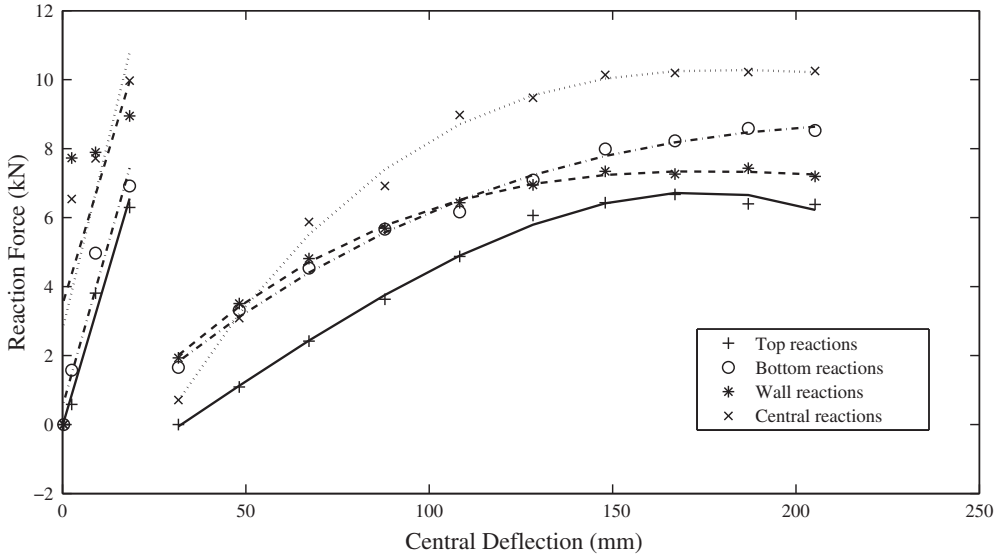

Fig. 14. Out of plane reactions on individual panel sides for Experiment 2. The edge locations are shown in Fig. 11.

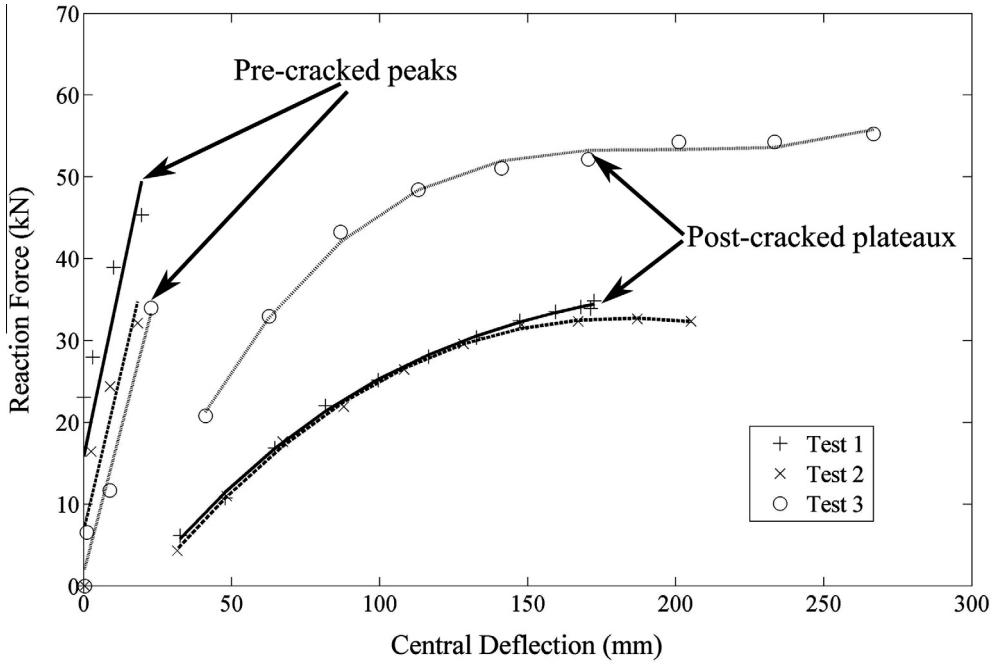

Fig. 15. Total out of plane reactions forces for all experiments. The pre-cracked peaks at low deflections are apparent.

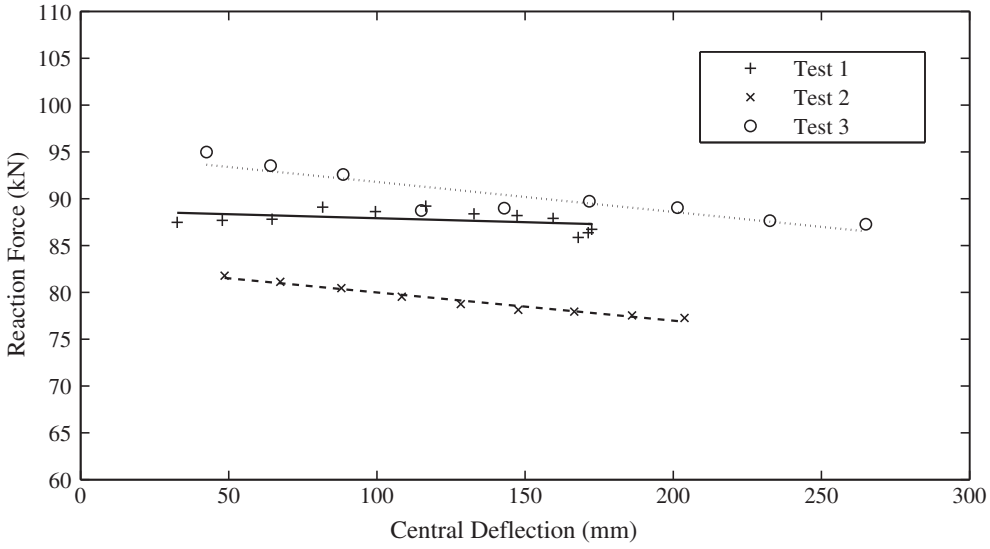

Fig. 16. Total in plane reactions for all three experiments.

Table 4
Summary of the pre-cracked out-of-plane peaks and out-of-plane and in-plane plateaux for the blasts considered.

Experiment	Out-of-plane pre-crack reactions peak (kN)	Out-of-plane post crack plateau (kN)	In-plane post crack plateau (kN)
1	45	33	88
2	32	32	79
3	34	53	90

4. Discussion

The analyses performed in this study rely on several key assumptions. However, it is possible to assess their reliability considering some of the results shown.

When considering the pre-crack results, it was noted that the proportions of bending and axial force plots shown in Fig. 7 correlate with the deflected shape observed during the experiments. The pane exhibits most strain near the edges, being relatively flat in the central area, especially at earlier time points. This would indicate that most of the bending strains would also be concentrated along the edges, which is confirmed by the FEA results. Fig. 8 again confirms this result, showing far higher stresses near the edges. This was not just the result of applying the FEA proportions to the raw data. Fig. 18 shows a total strain plot in a similar location and time step as those used for Fig. 8, where again the increases in strains at the edges can be seen.

The axial forces proved to be small. Whilst their magnitude had to be considered given the large deflection, it is doubtful whether their contribution is significant, especially when the large

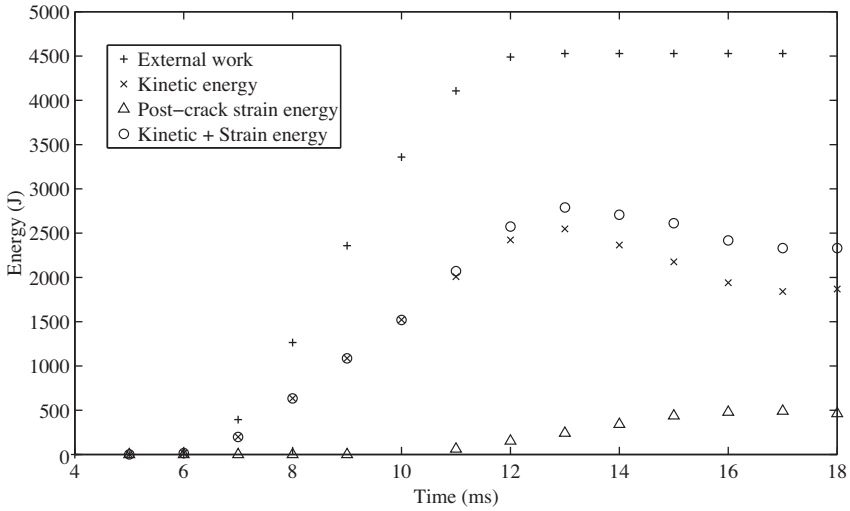

Fig. 17. External work done by the pressure, glazing kinetic energy and internal PVB strain energy estimates for Experiment 2.

Table 5
Energy results for the three experiments. The work done was based on the applied pressure and the window deflections at each point. The strain energy was assumed to be the strain energy of the PVB after glass cracking. The kinetic energy was calculated with the DIC velocity measurements and the mass of the glazing at each facet. The lost energy through irreversible deformations was assumed to be the difference between the kinetic and strain energy and the total work done.

Experiment	Work done (J)	Kinetic energy (J)	Strain energy (J)	Kinetic + Strain energies (J)	Energy lost through cracking and delamination (J)	Energy lost through cracking and delamination (%)
1	2350	607	530	1137	1213	52
2	4530	1870	460	2330	2200	49
3	6260	4165	755	4920	1340	21

Table 6
Comparison of the estimated blast energy with the work done and the energy lost through irreversible deformations. The blast energy is based on the explosive quantities, the stand-off and the window size. The other quantities are as per Table 5.

Experiment	Blast energy–spherical front (J)	Blast energy–hemispherical front (J)	Work done (J)	Kinetic + Strain energy (J)	Energy lost through cracking and delamination (J)
1	53,400	106,800	2350	1137	1213
2	70,500	141,000	4530	2330	2200
3	92,100	184,200	6260	4920	1340

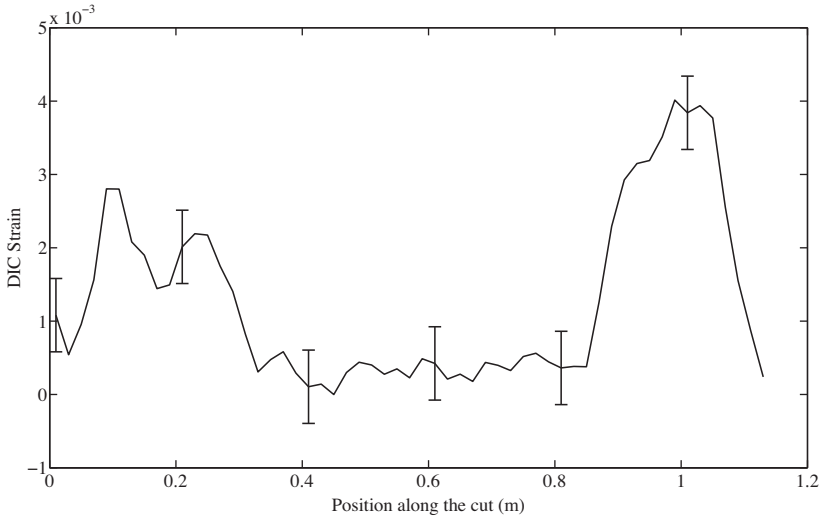

Fig. 18. DIC strains along a cut in Experiment 2. DIC uncertainties of 0.1% were assumed to plot the data error bars. The error bars were plotted at only a few points for clarity.

uncertainties of the analysis are considered. Specifically, the noise in the data in this phase was fairly high. The uncertainty in the DIC strain measurements was in the order of 100 microstrains, which was a significant percentage of the observed strains before the failure of the glass. The filtering shown in Fig. 8 reduced this effect. However it could not eliminate it completely at all points. Given the vast quantity of data to be processed, an automated system was employed. The filtering and the averaging over the last few

data points reduced the variability of the data along each edge, as can be seen in Fig. 9, however this could not be completely eliminated. It was therefore difficult to decide to what extent each individual datum can be considered accurate beyond an order of magnitude level.

The issue of small recorded strains was less significant for the post-crack analysis. In this case however one of the major issues was the material model employed to calculate the reactions. Hooper [1] employed the Johnson–Cook model for his FEA model. Whilst this did not represent the theoretical physical behaviour of the material, it did show a similar trend, as seen in the recorded data. It is hypothesised that the plateaux in the cracked laminated glass stresses were caused by the delamination of the glass fragments from the PVB membrane. This complex behaviour was of course very different from plasticity in metals. However the final stress strain curves were similar, hence justifying the adoption of the model equation. The plateau stresses calculated here were between 10 and 15 MPa. This was comparable to the measurements obtained through Hooper et al.'s laboratory experiments, giving credence to the results described. However, the laboratory results were not directly employed as the material properties might be heavily dependent on crack spacing and other cracked laminate characteristics. The fit therefore had to be performed again for the available blast data.

The uncertainties also affected the energies calculation. It was decided that the pre-crack bending and membrane strain energies could not be usefully calculated with the present data, as the noise present would have precluded sufficiently precise estimates for comparisons with other energy quantities. The calculation of the post-crack internal strain energy was also significantly simplified. In theory, it might have been possible to include the energy loss due to the non-linear composite properties directly at this stage by using the fitted material properties to the DIC data. However, it was decided that the uncertainties in the data would have been too large to produce accurate results. Instead, it was preferred to only directly account for the elastic behaviour of the material with constant stress throughout each strip considered. The non-linearity of the real composite material behaviour therefore would partially account for the differences between the work done and the kinetic and strain energies found. Whilst the exact energy estimates, especially before the glass cracking, will be subject to similar uncertainties as the reaction forces, the result presented is useful as it explicitly shows that a significant portion of the energies applied can be absorbed by the samples, an important factor in the design of these elements.

The results of the various experiments showed interesting trends. The pre-cracked peaks varied to a lesser extent than the post-cracked plateaux between the experiments. This was most likely due to the inherent capacity of the glass plies which, as their make-up and dimensions were identical, would have fractured at approximately the same deflection. The greater variation of the post-cracked reactions was due to the different characteristics of the blast waves, as these all presented different peak pressures and impulses. In all experiments though, these reactions clearly approached a plateau level. This behaviour was similar to what was observed when considering the cracked glass stress strain curves, linking these two aspects. The energy calculations also showed that a significant proportion of the external work done on the window was dissipated through irreversible deformations, such as the glass cracking and the progressive delamination of glass fragments from the PVB membrane. For example, whilst as mentioned above the data before the glass cracking was not precise enough for a direct calculation, the FEA analyses performed for the pre-crack reaction calculations indicated that approximately 500 J would be absorbed by the glass layers strain energy. This would then be dissipated upon the failure of the glass plies. Additionally, 10%–20% of the work done by the pressure on the panels is absorbed by the PVB as strain energy. A portion of this will be in the form of irrecoverable plastic deformations, increasing further the dissipated energy. This result is similar to what was observed by Hidallana-Gamage et al. [19], who reported the PVB energy absorption in their FEA model as 12%–16% of the total.

The comparison between the total blast energy, the work done and the energy absorbed by the system showed that most of the energy is reflected or vented around the structure, with a maximum of 6.8% transferred to the glazing system. The energy absorbed by material failures was also small, with a maximum of 3.1% in Experiment 2. This result indicates that the absorption capability of the system is relatively small compared to the energies which are potentially applied to it. In the experiments performed by Hooper the set up design allowed most of pressure wave to escape around the structure, limiting damage to the specimens at the same time as potentially increasing damage to surrounding elements. It is possible that in a larger façade this venting would not be possible and the window system would need to be designed to be more compliant and able to absorb a greater amount of energy. More flexible façade systems would be advantageous for this and would at the same time reduce the blast energy available to damage other structures further away from the blast.

A marked difference was observed between the in-plane and the out-of-plane post-cracked results. Whilst the out-of-plane forces rose gradually, the in-plane reactions increased very quickly to their plateau levels. As the overall forces were almost constant, the increased steadiness of the in-plane reactions was an effect of the geometric variations of the glass angles θ. Whilst the out-of-plane reactions were proportional to $\sin\theta$, the in plane reactions were proportional to $\cos\theta$. This tended to vary much more slowly at the angles recorded, which were in the region of 0°–30°. This would not only explain the increase in stability of the forces, but also why the in-plane reactions tended to decrease. With increasing angles, a larger proportion of the force would be out-of-plane, producing a small but noticeable decrease of the calculated in-plane reactions.

5. Conclusion

In this paper the available experimental data were employed to calculate reaction forces along the edges of the glazing panels. Pre-cracked reactions were estimated using a finite element model to separate bending moment and membrane force contributions to strains from the total deformations measured with DIC. These components were then calculated and reaction forces found. The post-crack reactions were found using the DIC strains, assuming that only membrane forces would be acting in this phase. A material model for the cracked laminate was fitted using the strain gauge data and DIC strains in the region at the centre of each panel side. This was then used to convert DIC strains along all the edges into stresses. The results were used to calculate the proportion of energy which was absorbed by non-recoverable deformations.

The out-of-plane reactions showed a distinct early peak before glass failure. This seemed to be of a similar magnitude in the cases considered. It was hypothesised that the size of this force was related to the geometric properties of the panel and hence to the maximum forces which could be resisted by the glass before shattering.

The post-cracked reactions reached a distinct plateau as the central deflections increased. This is compatible with the observed behaviour of the cracked laminate composite material, which showed a plateau in its stress strain data. One possible cause for this was the delamination between the PVB interlayer and the outer glass plies, which tended to detach as the strains increase. This observation was also supported by the energy calculations,

which showed that a significant proportion of the external work was absorbed by irreversible phenomena.

The results obtained in this paper are being used to improve the resistance function of this kind of pane for the single degree of freedom system design method. This enables more precise designs, improving both the safety and the efficiency of glazing systems.

Acknowledgements

The authors acknowledge the Engineering and Physical Sciences Research Council (EPSRC) and Arup Resilience, Security and Risk for financially supporting Dr Paolo Del Linz during his PhD and Dr Paul A. Hooper during his PhD. The authors also thank the Centre for the Protection of National Infrastructure (CPNI) for providing access to the GL Group test facilities at RAF Spadeadam.

References

[1] Hooper PA, Sukhram RAM, Blackman BRK, Dear JP. On the blast resistance of laminated glass. Int J Solids Struct 2012;49:899–918.
[2] Stephens RAC. Determination of the resistance of laminated glass subjected to blast loading using high speed video [M.Sc. thesis]. Cranfield University; 2008.
[3] Wei J, Dharani LR. Fracture mechanics of laminated glass subjected to blast loading. Theor Appl Fract Mech 2005;44:157–67.
[4] Wei J, Dharani LR. Response of laminated architectural glazing subjected to blast loading. Int J Impact Eng 2006;32:2032–47.
[5] Kumar P, Shukla A. Dynamic response of glass panels subjected to shock loading. J Non Cryst Solids 2011;357:3917–23.
[6] Larcher M. Simulation of laminated glass loaded by air blast waves. In: Ninth international conference on the mechanical and physical behaviour of materials under dynamic loading, Brussels, Belgium; 7–11 September 2009. p. 1553–9.
[7] Zhang X, Hao H, Ma G. Parametric study of laminated glass window response to blast loads. Eng Struct 2013;56:1707–17.
[8] Smith D. Glazing for injury alleviation under blast loading—United Kingdom practice. In: Glass processing days, Tampere; 2001. p. 335–40.
[9] Biggs JM. Introduction to structural dynamics. USA: McGraw-Hill Publishing Company; 1964.
[10] Fischer K, Häring I. SDOF response model parameters from dynamic blast loading experiments. Eng Struct 2009;31:1677–86.
[11] Hooper P. Blast performance of silicone-bonded laminated glass [Ph.D. thesis]. Imperial College; 2011.
[12] Dassault Systèmes Simulia Corp. Abaqus analysis manual v6.9. Providence, RI; 2009.
[13] Rivlin RS. Large elastic deformations of isotropic materials. I. Fundamental concepts. Philos Trans R Soc Lond Ser A Math Phys Sci 1948;240:459–90.
[14] Meunier L, Chagnon G, Favier D, Orgéas L, Vacher P. Mechanical experimental characterisation and numerical modelling of an unfilled silicone rubber. Polym Test 2008;27:765–77.
[15] Rose TA. An approach to the evaluation of blast loads on finite and semi-infinite structures [Ph.D. thesis]. Cranfield University; 2001.
[16] Cormie D, Mays G, Smith P. Blast effects on buildings. 2nd ed. London: ICE Publishing; 2009.
[17] Johnson GR, Cook WH. A constitutive model and data for metals subjected to large strains* high strain rates and high. In: Proceedings of the seventh international symposium ballistic. Netherlands: The Hague; 1983. p. 541–7.
[18] Jones H, Miller AR. The detonation of solid explosives: the equilibrium conditions in the detonation wave-front and the adiabatic expansion of the products of detonation. Proc R Soc Lond A Math Phys Sci 1948;194:480–507.
[19] Hidallana-Gamage HD, Thambiratnam DP, Perera NJ. Failure analysis of laminated glass panels subjected to blast loads. Eng Fail Anal 2014;36:14–29.